# Fusion of Evidences for Edge Detection in PolSAR Images

Anderson A. de Borba
*Dept. Engenharia Elétrica e Computação*
*UPM – Universidade Presbiteriana Mackenzie*
IBMEC-SP
São Paulo, Brazil
anderson.borba@ibmec.edu.br

Maurício Marengoni
*Dept. Engenharia Elétrica e Computação*
*UPM – Universidade Presbiteriana Mackenzie*
São Paulo, Brazil
mauricio.marengoni@mackenzie.br

Alejandro C. Frery
Laboratório de Computação Científica e Análise Numérica- LACCAN
*UFAL – Universidade Federal de Alagoas*
Maceió, Brazil
acfrery@laccan.ufal.br

***Abstract*—Polarimetric Synthetic Aperture Radar (PolSAR) has achieved an important position as a remote sensing imaging method. However, PolSAR images are contaminated with speckle noise, making its processing and analysis challenging tasks. The present study discusses a detection method based on the fusion of evidences obtained in the intensity channels of multilook PolSAR images. The method consists of detecting transition points in the finest strip of data which spans two regions using the maximum likelihood. This is applied to each of the three intensity channels (hh), (hv) and (vv). The fusion methods are simple average, stationary wavelet transform (SWT), principal component analysis (PCA), and ROC statistics. The results indicate improvement performance of the approach in detecting edges with possible paths for future research.**

***Index Terms*—PolSAR, edge detection, maximum likelihood estimation, fusion**

## I. Introduction

This work presents results on the detection and fusion of edge evidence applied to Polarimetric Synthetic Aperture Radar images (PolSAR). Models and algorithms as required for appropriate treatment of their special statistical characteristics were employed.

Among the available edge detection techniques for SAR imagery, it is worth mentioning those based on the gradient, Refs. [1]–[4], and on Markov chains, Ref. [5]. The former suffers from the effect of speckle, and the latter leads to computer-intensive methods. Ref. [6] presents a comparison between several edge detectors.

Alternatively, techniques based on statistical modeling have been used in edge detection, Refs. [6]–[9] and, more recently, utilizing *Deep Learning*, Refs. [10]–[13].

This work relies on ideas stemming from information fusion. This approach has been followed by Refs. [14], [15] in order to extract valuable knowledge from remotely sensed data.

This paper follows the statistical modeling approach, mainly the techniques described in Refs. [8], [16] using the Wishart distribution. The basis for the fusion of information is described in Refs. [15], [17].

The objective of this work shows the viability of a procedure for edge detection in each channel of a PolSAR image and then performed the fusion of evidences. The intent is understanding and quantifying the importance of the information provided by each channel in order to better edge detection.

The article is structured as follows: Section II describes the statistical modeling for PolSAR data, its use is presented in Sections III, IV, V, and VI. Section VII describes the fusion of edge evidence approaches with an emphasis on the ROC statistics-based method. Numerical results are shown and analyzed in Section VIII and, finally, Section IX concludes the paper with remarks, future research directions and, the viability to detect edges in each channel of a PolSAR image.

## II. Statistical modeling for PolSAR data

Fully polarimetric SAR systems transmit orthogonally polarized microwave pulses and measure orthogonal components of the received signal. For each pixel, there is a matrix of scattering coefficients, which are complex numbers and describe the transformation from the transmitted electromagnetic field to the received electromagnetic field.

The transformation can be represented as

$$\begin{bmatrix} E_{\mathrm{h}}^{\mathrm{r}} \\ E_{\mathrm{v}}^{\mathrm{r}} \end{bmatrix} = \frac{e^{\hat{\imath}kr}}{r} \begin{bmatrix} S_{\mathrm{hh}} & S_{\mathrm{hv}} \\ S_{\mathrm{vh}} & S_{\mathrm{vv}} \end{bmatrix} \begin{bmatrix} E_{\mathrm{h}}^{\mathrm{t}} \\ E_{\mathrm{v}}^{\mathrm{t}} \end{bmatrix},$$

where $k$ denotes the wave number, $\hat{\imath}$ is the complex unit, and r is the distance between the radar and the target. The electromagnetic field with components $E_{\mathrm{i}}^{\mathrm{j}}$ has a subscribed index denoting horizontal (h) or vertical (v) polarization, while the superscript index indicates the received (r) or transmitted (t) wave. Defining $S_{\mathrm{ij}}$ as the complex scattering coefficients, such that the indexes i and j are associated with the reception and transmission of waves, for example, the scattering coefficient

978-1-7281-4072-1/19/$31.00 

$S_{\text{hv}}$ is associated with the wave transmitted in the vertical direction (v) and received in the horizontal direction (h).

The complex scattering matrix $\mathbf{S}$ is defined by

$$\mathbf{S} = \begin{bmatrix} S_{\text{hh}} & S_{\text{hv}} \\ S_{\text{vv}} & S_{\text{vv}} \end{bmatrix}, \tag{1}$$

and if the medium of propagation of waves is reciprocal, then the reciprocity theorem, Ref. [18], allows to state the scattering matrix as being Hermitian. In this way, the scattering matrix (1) can be represented by the vector $\mathbf{s} = [S_{\text{hh}}, S_{\text{hv}}, S_{\text{vv}}]^T$.

Following Refs. [19], [20], the distribution of $\mathbf{s}$ is assumed to be Gaussian circular complex multivariate with zero mean $N_3^{\mathbb{C}}(0, \mathbf{\Sigma})$, and probability density function (pdf) given by:

$$f_{\mathbf{s}}(\mathbf{s}; \mathbf{\Sigma}) = \frac{1}{\pi^3 |\mathbf{\Sigma}|} \exp(-\mathbf{s}^H \mathbf{\Sigma}^{-1} \mathbf{s}), \tag{2}$$

where $|\cdot|$ is the determinant, the superscript index $H$ denotes the conjugate complex number, and $\mathbf{\Sigma}$ is the covariance matrix of $\mathbf{s}$ such that $\mathbf{\Sigma} = E[\mathbf{s}\mathbf{s}^H]$, where $E[\cdot]$ denotes the expected value.

This statistical modeling has been confirmed for a variety of the polarimetric SAR data, and it contains all the necessary information to characterize the backscatter according to Refs. [21], [22]

The statistical modeling described so far deals only with single-look modeling. However, polarimetric images are usually subjected to multilook processing in order to improve the signal-to-noise ratio. For this purpose, Refs. [19], [23] show that estimated positive definite Hermitian matrices are obtained by computing the average of $L$ independent samples of the same scene, resulting in the estimated sample covariance matrix:

$$\mathbf{Z} = \frac{1}{L} \sum_{\ell=1}^{L} \mathbf{s}_\ell \mathbf{s}_\ell{}^H, \tag{3}$$

where $\mathbf{s}_\ell$, $\ell = 1, \ldots, L$, are $L$ independent samples of complex vectors distributed as $\mathbf{s}$. The sample covariance matrix associated with $\mathbf{s}_\ell$ denotes the scattering for each of the $L$ looks.

## III. Multilook Wishart density function

Multilooked data follow a Wishart distribution with probability density function defined by:

$$f_{\mathbf{Z}}(\mathbf{Z}; \mathbf{\Sigma}_{\mathbf{s}}, L) = \frac{L^{mL} |\mathbf{Z}|^{L-m}}{|\mathbf{\Sigma}_{\mathbf{s}}|^L \Gamma_m(L)} \exp(-L \operatorname{tr}(\mathbf{\Sigma}_{\mathbf{s}}{}^{-1} \mathbf{Z})), \tag{4}$$

where, $\operatorname{tr}(\cdot)$ is the trace operator of an array, $\Gamma_m(L)$ is a multivariate Gamma function defined by

$$\Gamma_m(L) = \pi^{\frac{1}{2}m(m-1)} \prod_{i=0}^{m-1} \Gamma(L-i),$$

and $\Gamma(\cdot)$ is the Gamma function. In this study, $m = 3$ is considered. This situation is denoted by $\mathbf{Z} \sim W(\mathbf{\Sigma}_{\mathbf{s}}, L)$, which satisfies $E[\mathbf{Z}] = \mathbf{\Sigma}_{\mathbf{s}}$. Since there is no ambiguity, $\mathbf{\Sigma}$ instead of $\mathbf{\Sigma}_{\mathbf{s}}$ is used to represent the covariance matrix associated with $\mathbf{S}$.

## IV. Edge Detection

Most of the usual techniques for edge detection, e.g., Sobel, Canny, Laplacian of Gaussian (LoG) and pyramidal LoG, assume additive Gaussian noise and, thus, they are ineffective for PolSAR imagery. The noise in these kinds of images is multiplicative, making edge detection in SAR images a challenging task.

The main idea for edge detection is based on Ref. [7], [16] and show how to detect the transition point in a thin strip between two regions of the image. The transition point is considered as edge evidence.

The following procedure is proposed:

1) identify the centroid of a region of interest (ROI) in an automatic, semi-automatic or manual manner;
2) cast rays from the centroid to the outside of the area;
3) collect data around the rays using the Bresenham's midpoint line algorithm, ideally the size of a pixel;
4) detect points in the data strips which provide evidence of changes in their statistical properties, i.e., a transition point that defines edge evidence;
5) use the Generalized Simulated Annealing (GenSA) method, Ref. [24], to find maximum points in the functions of interest;
6) fuse the evidence of detected edges in the hh, hv and vv channels.

With this, fully polarized data is not required, only the intensity channels.

## V. Maximum Likelihood Estimator (MLE)

Suppose $\mathbf{X} = (X_1, X_2, \ldots, X_n)^T$ is a random vector distributed according to the probability density function $f(\mathbf{x}, \theta)$ with parameters $\theta = (\theta_1, \ldots, \theta_d)^T$ in the parameter space $\Theta$. The likelihood function is

$$L(\theta; \mathbf{X}) = \prod_{i=1}^{n} f(x_i; \theta),$$

and the logarithmic likelihood function, which is also called the log-likelihood function is

$$\ell(\theta; \mathbf{X}) = \ln L(\theta; \mathbf{X}) = \sum_{i=1}^{n} \ln f(x_i; \theta). \tag{5}$$

A maximum likelihood estimator is any point in $\Theta$ satisfying $\widehat{\theta} = \arg\max_{\theta \in \Theta} L(\theta; \mathbf{x})$ or, equivalently, $\widehat{\theta} = \arg\max_{\theta \in \Theta} \ell(\theta; \mathbf{x})$.

Consider now that the sample $\mathbf{Z}^T = (\mathbf{Z}_1, \mathbf{Z}_2, \ldots, \mathbf{Z}_N)$ is split into two: $\mathbf{Z}_1, \ldots, \mathbf{Z}_j$ and $\mathbf{Z}_{j+1}, \ldots, \mathbf{Z}_j$. These parts may belong to two different Wishart distributions: those characterized by $\mathbf{\Sigma}_{\mathbf{A}}$, and $\mathbf{\Sigma}_{\mathbf{B}}$, both with the same number of looks $L$. Finding the edge consists of finding the point $j$ (or $j+1$) that separates them.

Finding the edge $j$ by maximum likelihood can be achieved by looking for the position $\widehat{j}$ that maximizes the likelihood equation of the two samples:

$$L(j) = \prod_{k_1=1}^{j} f_{\mathbf{Z}}(\mathbf{Z}_{k_1}; \widehat{\mathbf{\Sigma}}_{\mathbf{A}}, L) \prod_{k_2=j+1}^{N} f_{\mathbf{Z}}(\mathbf{Z}_{k_2}; \widehat{\mathbf{\Sigma}}_{\mathbf{B}}, L), \tag{6}$$

where $\widehat{\mathbf{\Sigma}}_{\mathbf{A}}$ is the maximum likelihood estimator of $\mathbf{\Sigma}_{\mathbf{A}}$ based on the sample $\mathbf{Z}_1, \ldots, \mathbf{Z}_j$, and $\widehat{\mathbf{\Sigma}}_{\mathbf{B}}$ is the maximum likelihood estimator of $\mathbf{\Sigma}_{\mathbf{B}}$ based on the sample $\mathbf{Z}_{j+1}, \ldots, \mathbf{Z}_N$. Analogously, one may optimize with respect to $j$ the log-likely function, i.e., finding where

$$\ell(j) = \sum_{k_1=1}^{j} \ln f_{\mathbf{Z}}(\mathbf{Z}_{k_1}; \widehat{\mathbf{\Sigma}}_{\mathbf{A}}, L) + \sum_{k_2=j+1}^{N} \ln f_{\mathbf{Z}}(\mathbf{Z}_{k_2}; \widehat{\mathbf{\Sigma}}_{\mathbf{B}}, L). \tag{7}$$

is maximum with respect to $1 \leq j \leq N$. The point that solves this optimization problem is denoted $\widehat{j}$.

The estimates for the covariance matrices can be found using the maximum likelihood estimator denoted by $\widehat{\Sigma}$, Ref. [19]:

$$\widehat{\mathbf{\Sigma}_I}(j) = \begin{cases} j^{-1} \sum_{k=1}^{j} \mathbf{Z}_k & \text{if} \quad I = A, \\ (N-j)^{-1} \sum_{k=j+1}^{N} \mathbf{Z}_k & \text{if} \quad I = B. \end{cases} \tag{8}$$

After algebraic manipulations on each term of the summation using the equation (8), it is obtained:

$$\begin{aligned} \ell(j) &= N\left[mL(\ln L - 1) - \ln \Gamma_m(L)\right] \\ &\quad - L\left[j \ln |\widehat{\mathbf{\Sigma}}_A(j)| + (N-j) \ln |\widehat{\mathbf{\Sigma}}_B(j)|\right] \\ &\quad + (L-m) \sum_{k=1}^{N} \ln |\mathbf{Z}_k|. \end{aligned} \tag{9}$$

The argument of the maximum $\widehat{j}$ is the edge evidence that will be used in our fusion methods.

## VI. Application in simulated images

The methodology (MLE) for detecting edge evidence will be applied to a simulated image based on Refs. [16], [25]. The image has $400 \times 400$ pixels and is composed of two samples obeying the Wishart distribution; cf. Fig. 1(a).

For each pair of covariance matrices $\Sigma_{k_1}$, $\Sigma_{k_2}$ a PolSAR image $I_{k_1,k_2}$ is simulated: samples of $W_G(\Sigma_{k_1}, 4)$ in the left half, and samples of $W_G(\Sigma_{k_2}, 4)$ in the right half. The image has $400 \times 400$ pixels.

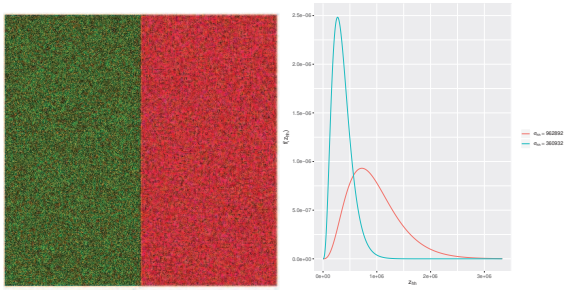

(a) Pauli decomposition (b) Marginal densities of the hh channel

Fig. 1. Edges evidences

The Pauli decomposition is based on the linear combination of intensity channels: $(\mathbf{I}_{\text{hh}} + \mathbf{I}_{\text{vv}}, \mathbf{I}_{\text{hh}} - \mathbf{I}_{\text{vv}}, \mathbf{I}_{\text{hv}})$. This decomposition shows the evidence of edge in the middle line, as presented in Fig. 1(a).

Fig. 1(b). shows the density function of $\sigma_{\text{hh}}$ with parameters extracted from real data for forest and urban areas: $\sigma_{\text{hh}} = 962892$ and $\sigma_{\text{hh}} = 360932$.

(a) Channel hh (b) Channel hv (c) Channel vv

Fig. 2. Edges evidences

The functions have a peak indicating the evidence of the edge that should be captured, but the functions are not smooth, hindering the use of optimization methods that require the calculation of the derivative. This problem was solved using Generalized Simulated Annealing (GenSA) [24], suitable for non-differentiable functions.

The error is measured simulating 400 independent images and finding $\widehat{j}$ in a line fixed. By construction, the vertical line 200 is considered as the real edge in each replication, so the error for this replication is the absolute value of the difference between this point and the estimated value, and it is computed by $E(r) = |200 - \widehat{j}(r)|$, $1 \leq r \leq 400$.

Relative frequencies to estimate the probability of having an error smaller than a number of pixels is used. Denoting $H(k)$ the number of replications for which the error is less than $k$ pixels, an estimate of this probability is $f(k) = \frac{H(k)}{400}$. In the tests performed in this section, $k$ varies between 1 and 10. The algorithm is described in Ref. [8]. Fig. 3 shows these probabilities as computed in each channel $I_{\text{hh}}$, $I_{\text{hv}}$ and $I_{vv}$ of the image.

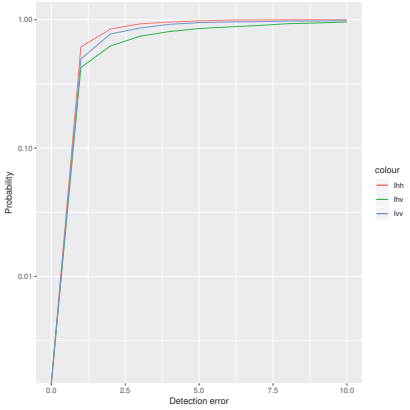


Fig. 3. Probability of detecting edges evidences.

## VII. Methods of fusion of edge evidence

### A. Simple average

The simple average fusion method proposes the arithmetic mean of the edge evidence in each channel. The edge evidence fusion can be calculated by

$$IF(x,y) = \frac{1}{nc}\sum_{i=1}^{nc} IE_i(x,y), \tag{10}$$

where $nc$ is the number of channels to be used in the fusion, $IE$ is image with edges evidences in each channel, and $IF$ is image fusion. More details are presented in Ref. [17].

### B. Stationary wavelet transform – SWT

This section is based on Ref. [26]. SWT filters are applied separately in vertical and horizontal directions and downsampled by a factor of two in the image $I$. In this way, the image is filtered by the low pass filter L and the high pass filter H in the horizontal direction and then downsampled by a factor of two to create the coefficients matrices $I_{\mathrm{L}}$ and $I_{\mathrm{H}}$. After this, the coefficients matrices $I_{\mathrm{L}}$ and $I_{\mathrm{H}}$ are again subjected to the low pass and high pass filters in the vertical direction and newly downsampled by a factor of two to create sub-images. $I_{\mathrm{LL}}$,$I_{\mathrm{LH}}$, $I_{\mathrm{HL}}$ and $I_{\mathrm{HH}}$. The SWT fusion method can be described by the following steps:

- calculate the SWT decomposition by getting $I_{\mathrm{HH}}$, $I_{\mathrm{HL}}$, $I_{\mathrm{LH}}$ and $I_{\mathrm{LL}}$ for each channel (image);
- in the decompositions $I_{\mathrm{HH}}$, obtain the arithmetic mean of all channels, pixel by pixel. In the decompositions $I_{\mathrm{HL}}$, $I_{\mathrm{LH}}$ and $I_{\mathrm{LL}}$, the maximum between each channel is found, pixel by pixel, leaving a new decomposition $\bar{L}_{\mathrm{HH}}$, $\bar{I}_{\mathrm{HL}}$, $\bar{I}_{\mathrm{LH}}$ and $\bar{I}_{\mathrm{LL}}$;
- perform the inverse SWT transformation. The image is obtained by fusing the edge evidence $IF(x,y)$.

### C. Principal component analysis – PCA

This section is based on Refs. [17], [26]. The method is comprised of the following steps:

- organize the data in such a way that each image has a column vector, forming a $Y$ matrix of dimension $l \times nc$, where $l = mn$, the lines times the columns of the matrices to be used in the fusion;
- calculate the average of the elements of these columns, generating a vector dimension of $1 \times nc$;
- subtract the average of each column from the $Y$ matrix, resulting in $X$, a matrix of the same dimension of $Y$;
- find $C$, the covariance matrix of $X$;
- calculate its eigenvalues $\Lambda$ and eigenvectors $D$, and sort the eigenvalues and eigenvectors in descending order. The matrices generated by the eigenvalues, on the main diagonal, and the eigenvectors placed in column, have dimensions $nc \times nc$;
- compute the components $P_i = {V_i}^{-1}\sum_{i=1}^{l} V_i$ with $i = 1,\ldots,nc$;
- fuse $IF(x,y) = \sum_{i=1}^{nc} P_i IE_i(x,y)$, recalling that $\sum_{i=1}^{nc} P_i = 1$.

### D. ROC statistics

The ROC method was proposed and described in [27], [28]:

- obtain the evidence of edges in the channels, and store it in $E_i$ matrices, with $i = 1,\ldots,nc$ in a binary way;
- define a $V$ edge frequency matrix. The $V$ matrix is generated by adding the evidence of $E_i$ edges;
- use thresholds ranging from $t = 1,\ldots,nc$ generating $M_t$ matrices;
- compare each $M_t$, fixed with all $E_i$, find the confusion matrix to generate the ROC curve. The point of the ROC curve closest (in the sense of the Euclidean distance) to the diagnostic line will have its threshold considered optimal;
- the $M_t$ matrix which corresponds to the threshold closest to the diagnostic line is the result of the fusion.

## VIII. Numerical results

The PolSAR image of the Flevoland region in the Netherlands is used, with $4$ looks, for the numerical tests. Fig. (4) shows the region of interest, with the radial lines for edge detection.

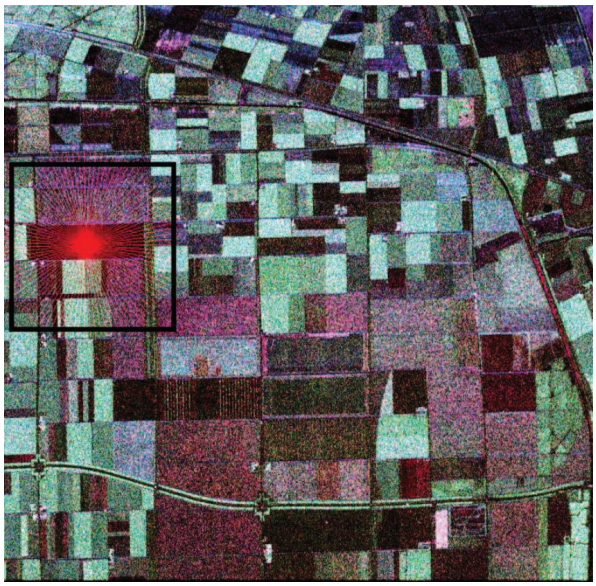

Fig. 4. Region of interest (ROI) in the image of Flevoland.

Figs. 5(a), (b) and (c) show, respectively, the edge evidence in the hh, hv and vv channels. The algorithm achieves better accuracy in channels hh and hv than in channel vv.

It is noteworthy that GenSA identified the maximum evidence correctly, even in the presence of multiple local maxima as in the case of the vv channel.

Figs. 6(a), (b), (c), and (d) show, respectively, the results of fusing these evidences. The methods use all the pixels detected in the three channels by using different weights: the average weights the pixels equally, SWT finds the coefficients of the

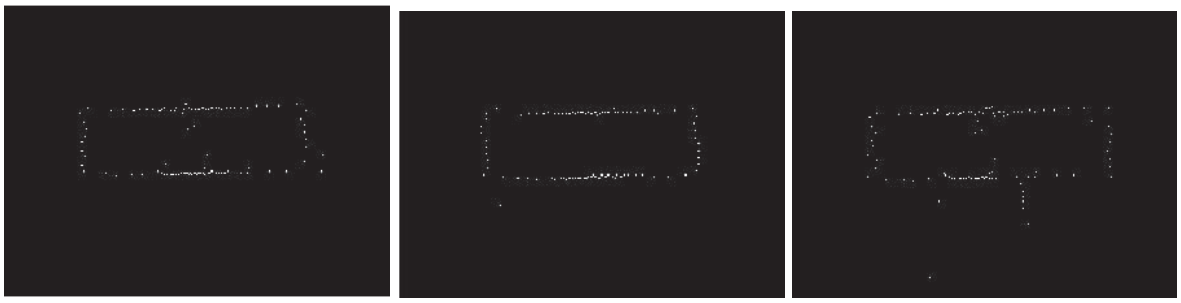

(a) Evidences in channel hh (b) Evidences in channel hv (c) Evidences in channel vv

Fig. 5. Edges evidences

linear combination of its wavelet bases, and PCA weights by the eigenvalues of the covariance matrix.

The ROC statistics method does not use all pixels of the channels, because the method is based on thresholds for discarding pixels. This was observed in Fig. 6(d).

## IX. Conclusion

In this article, methods for fusion of edges evidence in PolSAR images. First, edges evidence were found using the method of maximum likelihood in the three intensities channels. Second, fusion methods were applied, simple average, SWT, PCA, and ROC curve. A simulated image was used to quantify and compare the results.

The detection was performed by maximum likelihood, in which the function is not smooth and presents many local maximal. Therefore, the difficulty of using classical optimization methods was stressed. To solve this problem, Simulated Annealing was applied because it is appropriate to optimize non-differentiable functions.

The quality of the fusion with the probability of detecting the edge was correctly measured. There is an improvement in detecting evidence of edges in the intensity channels.

From the obtained results, the viability of increasing the number of channels used for edge evidence detection was identified, paving the way to research new fusion methods in PolSAR image.

## References


[1] R. Touzi, A. Lopes, and P. Bousquet, "A statistical and geometrical edge detector for sar images," *IEEE Transactions on Geoscience and Remote Sensing*, vol. 26, no. 6, pp. 764–773, Nov 1988.

[2] C. J. Oliver, D. Blacknell, and R. G. White, "Optimum edge detection in sar," *IEE Proceedings - Radar, Sonar and Navigation*, vol. 143, no. 1, pp. 31–40, Feb 1996.

[3] R. Fjortoft, A. Lopes, P. Marthon, and E. Cubero-Castan, "An optimal multiedge detector for sar image segmentation," *IEEE Transactions on Geoscience and Remote Sensing*, vol. 36, no. 3, pp. 793–802, May 1998.

[4] X. Fu, H. You, and K. Fu, "A statistical approach to detect edges in sar images based on square successive difference of averages," *IEEE Geoscience and Remote Sensing Letters*, vol. 9, no. 6, pp. 1094–1098, Nov 2012.

[5] F. Baselice and G. Ferraioli, "Statistical edge detection in urban areas exploiting sar complex data," *IEEE Geoscience and Remote Sensing Letters*, vol. 9, no. 2, pp. 185–189, March 2012.

[6] E. Girón, A. C. Frery, and F. Cribari-Neto, "Nonparametric edge detection in speckled imagery," *Mathematics and Computers in Simulation*, vol. 82, no. 11, pp. 2182 – 2198, 2012. [Online]. Available: http://www.sciencedirect.com/science/article/pii/S037847541200136X

[7] J. Gambini, M. Mejail, J. Jacobo-Berlles, and A. C. Frery, "Feature extraction in speckled imagery using dynamic B-spline deformable contours under the G0 model," *International Journal of Remote Sensing*, vol. 27, no. 22, pp. 5037–5059, 2006.

[8] A. C. Frery, J. Jacobo-Berlles, J. Gambini, and M. Mejail, "Polarimetric SAR image segmentation with b-splines and a new statistical model," *CoRR*, vol. abs/1207.3944, 2012.

[9] M. Horritt, "A statistical active contour model for sar image segmentation," *Image and Vision Computing*, vol. 17, no. 3, pp. 213 – 224, 1999. [Online]. Available: http://www.sciencedirect.com/science/article/pii/S0262885698001012

[10] J. E. Ball, D. T. Anderson, and C. S. Chan, "A comprehensive survey of deep learning in remote sensing: Theories, tools and challenges for the community," *CoRR*, vol. abs/1709.00308, 2017. [Online]. Available: http://arxiv.org/abs/1709.00308

[11] X. X. Zhu, D. Tuia, L. Mou, G. Xia, L. Zhang, F. Xu, and F. Fraundorfer, "Deep learning in remote sensing: A comprehensive review and list of resources," *IEEE Geoscience and Remote Sensing Magazine*, vol. 5, no. 4, pp. 8–36, Dec 2017.

[12] J. Pont-Tuset, P. Arbeláez, J. T. Barron, F. Marques, and J. Malik, "Multiscale combinatorial grouping for image segmentation and object proposal generation," *IEEE Transactions on Pattern Analysis and Machine Intelligence*, vol. 39, no. 1, pp. 128–140, Jan 2017.

[13] S. Xie and Z. Tu, "Holistically-nested edge detection," *Int. J. Comput. Vision*, vol. 125, no. 1-3, pp. 3–18, Dec. 2017. [Online]. Available: https://doi.org/10.1007/s11263-017-1004-z

[14] A. Samat, P. Gamba, S. Liu, Z. Miao, E. Li, and J. Abuduwaili, "Quad-polsar data classification using modified random forest algorithms to map halophytic plants in arid areas," *Int. J. Applied Earth Observation and Geoinformation*, vol. 73, pp. 503–521, 2018. [Online]. Available: https://doi.org/10.1016/j.jag.2018.06.006

[15] A. Salentinig and P. Gamba, "A general framework for urban area extraction exploiting multiresolution sar data fusion," *IEEE Journal of Selected Topics in Applied Earth Observations and Remote Sensing*, vol. 9, no. 5, pp. 2009–2018, May 2016.

[16] A. Nascimento, M. Horta, A. Frery, and R. Cintra, "Comparing edge detection methods based on stochastic entropies and distances for polsar imagery," *Journal of Selected Topics in Applied Earth Observations and Remote Sensing*, vol. 7, no. 2, pp. 648–663, 2014.

[17] H. Mitchell, *Image Fusion: Theories, Techniques and Applications*. Springer Berlin Heidelberg, 2010. [Online]. Available: https://books.google.com.br/books?id=D7DXAX6eH2oC

[18] J.-S. Lee and E. Pottier, *Polarimetric radar imaging: from basics to applications*. CRC press, 2009.

[19] N. R. Goodman, "The distribution of the determinant of a complex wishart distributed matrix," *Ann. Math. Statist.*, vol. 34, no. 1, pp. 178–180, 03 1963. [Online]. Available: http://dx.doi.org/10.1214/aoms/1177704251

[20] J. S. Lee, K. W. Hoppel, S. A. Mango, and A. R. Miller, "Intensity and phase statistics of multilook polarimetric and interferometric SAR im-

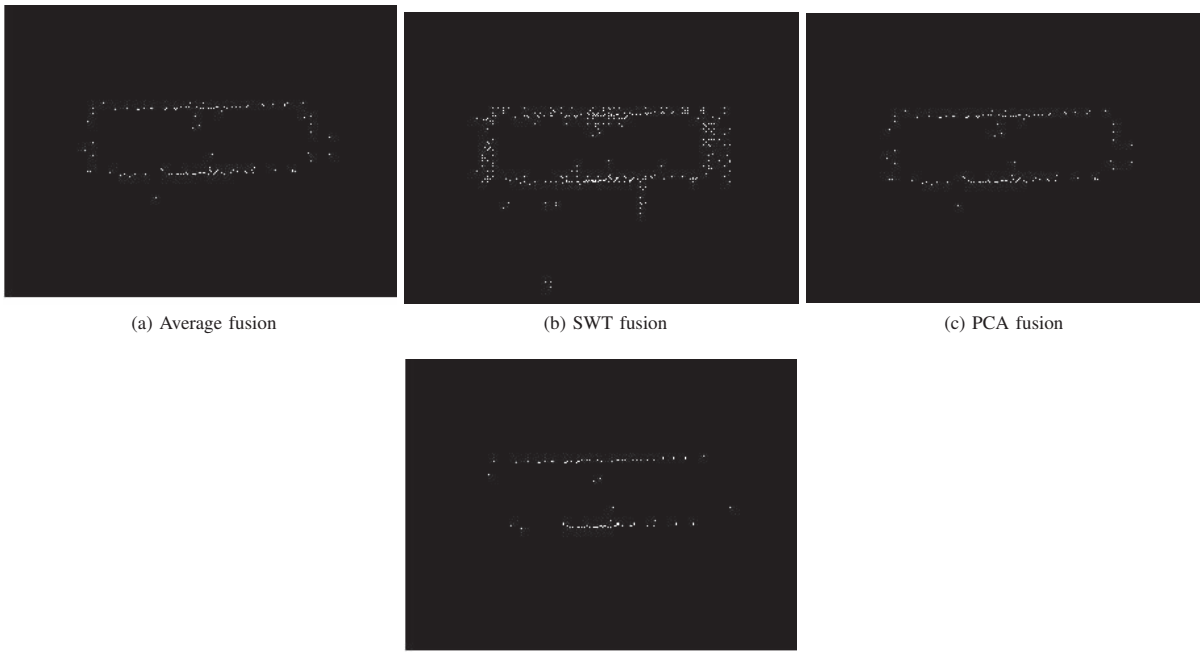

(a) Average fusion (b) SWT fusion (c) PCA fusion

(d) ROC fusion

Fig. 6. Fusion methods

agery," *IEEE Transactions on Geoscience and Remote Sensing*, vol. 32, no. 5, pp. 1017–1028, Sep. 1994.

[21] K. Sarabandi, "Derivation of phase statistics from the mueller matrix," *Radio Science*, vol. 27, 11 1992.

[22] C. López-Martínez, X. Fàbregas, and E. Pottier, "Multidimensional speckle noise model," *EURASIP Journal on Advances in Signal Processing*, vol. 2005, no. 20, p. 180956, Dec 2005. [Online]. Available: https://doi.org/10.1155/ASP.2005.3259

[23] S. N. Anfinsen, A. P. Doulgeris, and T. Eltoft, "Estimation of the equivalent number of looks in polarimetric synthetic aperture radar imagery," *IEEE Transactions on Geoscience and Remote Sensing*, vol. 47, no. 11, pp. 3795–3809, 2009.

[24] Yang Xiang, S. Gubian, B. Suomela, and J. Hoeng, "Generalized simulated annealing for efficient global optimization: the GenSA package for R." *The R Journal Volume 5/1, June 2013*, 2013. [Online]. Available: https://journal.r-project.org/archive/2013/RJ-2013-002/index.html

[25] L. Gomez, L. Alvarez, L. Mazorra, and A. C. Frery, "Fully polsar image classification using machine learning techniques and reaction-diffusion systems," *Neurocomputing*, vol. 255, pp. 52–60, 2017.

[26] V. Naidu and J. Raol, "Pixel-level image fusion using wavelets and principal component analysis," *Defence Science Journal*, vol. 58, no. 3, pp. 338–352, Mar. 2008. [Online]. Available: https://publications.drdo.gov.in/ojs/index.php/dsj/article/view/1653

[27] S. Giannarou and T. Stathaki, "Optimal edge detection using multiple operators for image understanding," *EURASIP Journal on Advances in Signal Processing*, vol. 2011, no. 1, p. 28, Jul 2011. [Online]. Available: https://doi.org/10.1186/1687-6180-2011-28

[28] T. Fawcett, "An introduction to roc analysis," *Pattern Recogn. Lett.*, vol. 27, no. 8, pp. 861–874, Jun. 2006. [Online]. Available: http://dx.doi.org/10.1016/j.patrec.2005.10.010